Non-conductive ferromagnets based on core double-shell nanocomposites for radio-electric applications

H. Takacs[1,2], B. Viala[1], V. Hermán[1], J.-H. Tortai[2], F. Duclairoir[3,4], J. Alarcon Ramos[1],
P.-H. Jouneau[3,4], H. Okuno[3,4] and G. Tallec[5]

helene.takacs@cea.fr

[1]CEA, LETI, MINATEC Campus, Grenoble, France
[2]LTM-CNRS-UJF, CEA, LETI, MINATEC Campus, Grenoble, France
[3]Univ. Grenoble Alpes, INAC, Grenoble, France – [4]CEA, INAC, Grenoble, France
[5]FEI Visualization Sciences Group, Mérignac, France

ABSTRACT

Two fabrication processes of magnetic metal-polymer nanocomposites are described (with and without radicals). Preservation of the net-moment of cobalt and electrical insulation are achieved by means of a core double-shell structure of cobalt-graphene-polystyrene. The maximum filling ratio is estimated at ~ 30%. The nanocomposites undergo percolation conductivity above ~ 2.4% but retain low conductivity (< 1 S/m) close to 30% leading to extremely low losses (10^{-3}) at high frequency. Ability for RF applications is discussed in regards to the obtained magnetization (0.6 - 0.9 T).

Keywords (5 max): nanocomposites, ferromagnetism, RF

1 INTRODUCTION

Polymer nanocomposites are attractive materials due to the ability to tailor final properties. They consist in nanometer fillers embedded in a matrix. The properties are controlled by the filler volume fraction. Composites are classified into diluted or percolated states [1]. With metallic fillers, the continuum percolation theory applies to the electrical conductivity [2]. Also dipolar-magnetism in interacting systems was reported [3].

In RF, polymer-metal nanocomposites are aimed to overcome the main obstacle of high-moment transition metals that are conductive. Recent works on nanocomposites of cobalt were reported but magnetization degradation was observed indicating that stable nanoparticles are needed [4, 5]. They can be protected with a shell that must be a protection against surface oxidation and spin-quenching especially with cobalt [6]. The shell thickness must be small as with core-shell structures, the percolation threshold dramatically decreases [7]. The thinnest coating capable to protect metallic nanoparticles belongs to Hayashi with the use of graphene layers [8]. From there, carbon-coated magnetic nanoparticles have emerged [9].

Now, the challenge is to convert such nanopowders into a processable material. Directly mixing nanoparticles and polymers is not an option as the resulting material has poor mechanical cohesion. Hence, particles need to be strongly bound to the polymer to get a cohesive structure. It was reported with Co/C grafted elastomers in [10]. In this work, we address non-covalent and covalent grafting of Co/C with polystyrene (PS). The key issue is to form ultra-thin PS shells
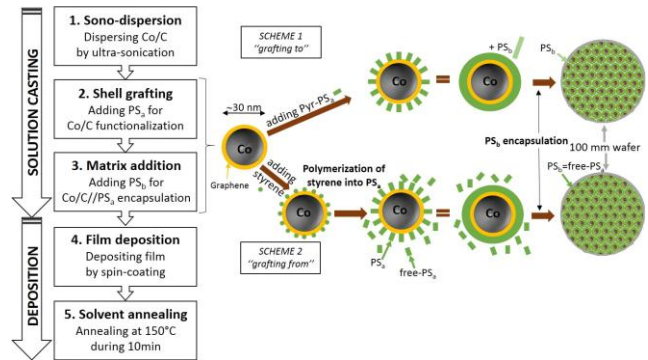
Figure 1: Flow chart and reaction schemes with grafting

(*i.e.* few nm) superimposed to the existing graphene coating (*i.e.* conductive) for electrical insulation and avoiding that the percolation threshold collapses. Turbobeads® (Sigma Aldrich) Co/C nanoparticles (30 nm in average) were used. A two-stage flow chart (Fig. 1) is explained with solution-casting and film-deposition. Three series of samples are considered with process variations. The nanoparticles weight fraction – and indirectly the volume fraction – was determined by Thermogravimetric Analysis (TGA). We report evidence of grafting between the two phases. The discussion addresses the filling limit, the conductive percolation and the impact of grafting on residual magnetization of cobalt. The tradeoff between electrical and magnetic properties is achieved.

2 EXPERIMENTAL DETAILS

The overall preparation was based on sonochemistry. Two grafting schemes were explored. *Scheme 1* was the radical-free option using non-covalent interactions based on electron sharing (*i.e.* π-π bonds). We used pyrene-terminated PS (*i.e.* Pyr-PS$_a$) whose electronic structure is close to that of graphene. *Scheme 2* used radicals to covalently graft PS to Co/C. The radicals originate from *in-situ* polymerization of monomers of styrene. Firstly, deagglomeration of Co/C powders is prerequisite. It was performed by sonication at 100 W during 10 min. Note that the duration of sonication must not exceed 30 min because graphene coating deteriorates for longer sonication times.

Series-A (chloroform formulation – scheme 1)
The formulation used initial weight m_i of 300 mg of Co/C in 8 mL of chloroform (CHCl$_3$) and 5 mg of Pyr-PS$_a$ (Polymer

Source) with low molecular weight M_w of 5.6 kg/mol aimed to form the polymeric shell (PS$_a$). The intermediate product is labeled Co/C//Pyr-PS$_a$-A. Subsidiary step is required to form the supporting matrix (PS$_b$). To do so, 2 mL of PS (0.75 g/mL, Sigma-Aldrich) with a higher M_w of 35 kg/mol were added to the solution. The reaction was stopped after 30 min of sonication. Series-A is labeled Co/C//Pyr-PS$_a$/PS$_b$-A.

Series-B (anisole formulation – scheme 1)
It is a variant of series-A using anisole (C$_7$H$_8$O) instead of CHCl$_3$ whose low boiling point T_b (*i.e.* 61.2°C) may be a limitation for applications. Anisole (T_b = 153.8°C) was aimed for spin-coating optimization. The solution casting was broader in composition with m_i varying from 100, 300, 500 to 700 mg. Labels are identical with replacing A by B.

Series-C (anisole formulation - scheme 2)
Scheme 2 is the radical option aimed to improve dispersion and cohesion. It is detailed in [11]. For practical reasons, m_i was limited to 100 mg. The reaction time is identical (*i.e.* 30 min). Two sub-schemes were considered: adding Co/C at the beginning of the reaction (*2a*) – with a lot of radicals – or at midterm (*2b*) – less radicals. Thus, we expect more PS$_a$ with *scheme 2a*. Conversely with *scheme 2b* more PS$_b$ is awaited with a higher output of unreacted free-PS. Here, free-PS replaces additional PS$_b$ (35 kg/mol) of *scheme 1*. Solution was precipitated in methanol to obtain a powder that was redispersed in anisole for spin-coating. Series-C is labeled Co/C//PS$_a$/PS$_b$-C (*2a* or *2b*).

Spin-coating required 1 mL of cast-formulations to deposit uniform μm-thick films on 4-inch oxidized silicon wafers. We used SPS SPIN200i-TT-PTFE spin processor. Films were solvent annealed at 150°C for 10 min at the end.

3 RESULTS AND DISCUSSION

3.1 Sedimentation time and spin-curves

Stabilized cast-solutions are required for spin-coating. Sedimentation study was conducted for Series-A after de-agglomeration, shell-grafting and matrix addition. Co/C are prone to agglomeration because of a non-null remanent magnetization at room temperature. With sonication a mixture of individual particles and clusters of ~ 100 nm was obtained, as measured by dynamic light scattering (DLS). Such suspension sediments after only 5 min.
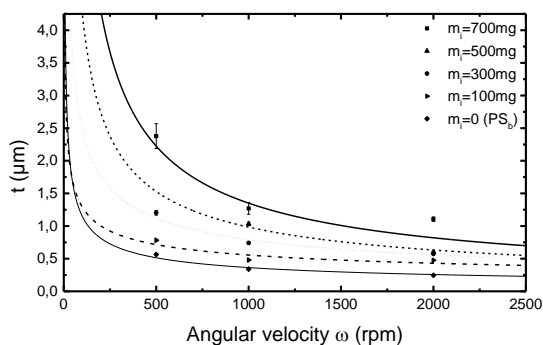
Figure 2: Full spin-curve established for Series-B
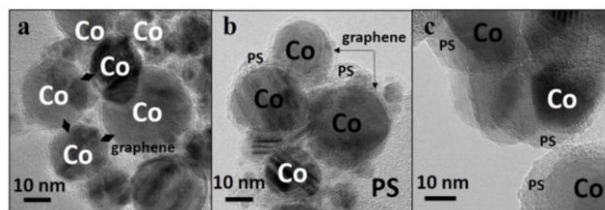
Figure 3: HR-TEM pictures of (a) deagglomerated Co/C particles, (b) Series-B and (c) Series-C 2b

When grafting the shell of Pyr-PS$_a$ and further embedding into the matrix of PS$_b$ sedimentation-time increases with 30 min and 75 min, respectively, due to steric hindrance.

Spin-coating is a known technique for homogeneous polymers and some emerging colloids [12]. However, there is no report with interacting magnetic suspensions. Before achieving reproducible films, the spinning parameters were optimized with Series-B over a broad range of composition. The spin-curves are shown on Fig. 2. The error bars are representative of the radial dispersion on 4" wafers. At first sight, the achieved thickness after solvent annealing agrees with the classical angular velocity dependence (*i.e.* $\propto \omega^{-0.5}$) of polymers, that is remarkable here. The tradeoff for ~ 1 μm-thick films was found at 1000 rpm with uniformity of ~ 5% indicating that radial and edge effects are weak.

3.2 Microstructure and thermal properties

The microstructure of nanocomposites is a complex feature that required a thorough investigation. HR-TEM images performed on FEI Osiris microscope at 200 kV are presented in Fig. 3. Fig. 3a shows deagglomerated Co/C nanoparticles. The graphene protective coating is well-visible with 8-10 layers (~ 5 nm). Series-B is presented in Fig. 3b. Graphene is unchanged, proving that *scheme 1* with no radical is safe. On the contrary, series-C does not display graphene contrast anymore (Fig. 3c). Complementary observations backed with Raman analysis revealed that graphene is much thinner and partially transformed into amorphous carbon [11]. Also Co$_3$O$_4$ traces were detected by XPS. Thus, *scheme 2* is more critical.

To deepen these visual observations, the glass transition temperature T_g was characterized by Differential Scanning Calorimetry (DSC). Series-B, C2a and C2b showed T_g at 68°C, 86°C and 88°C respectively which have to be compared to their own matrix. With *scheme 1*, PS$_b$ matrix exhibit T_g at 62°C while it is 75°C with *scheme 2*. Thus, with metallic fillers T_g is higher and the difference ΔT_g (*i.e.* 6°C (B), 11°C (C2a) and 13°C (C2b)) is large enough to be considered as an evidence of surface interactions [13]. Higher bond dissociation energies are consistent with the assumption of covalent grafting with *scheme 2*. Whether covalent or non-covalent, the chemical bonds are definitely strong enough to be irreversible.

3.3 Nanotomography and filling limits

Nanotomography is an automated serial sectioning technique for high resolution 3D visualization.
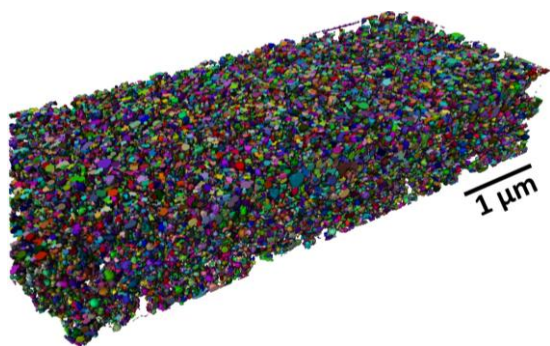
Figure 4: 3D image of series-A.
Image obtained with Avizo® software

Figure 5: Abacus of the maximum volume ratio x_v^M vs. shell thickness for different core sizes

It was performed on Series-A using Zeiss NVision 40 FIB/SEM dual beam instrument (400 slices of 3.5 nm). Images were denoised and the structure was skeletonized with Avizo® software. Fig. 4 shows the reconstructed volume after segmentation. Individual particles are well visualized. The volumetric structure is made of isolated closely-spaced nanoparticles and small clusters (~ 100 nm) that are homogeneously dispersed.

Besides weight fraction, one prefers to consider volume fraction, x_v, for applications as physical properties in composites are often percolative. The maximum value x_v^M is an important parameter. With core-shell structures, the shell-thickness is a key issue as x_v^M decreases when increasing shell-thickness and when decreasing core-size (Fig. 5). For a perfect triangular lattice of monodisperse spherical particles of unprotected Co particles x_v^M is 74%. With a perfect assembly of Co(50 nm)/C(5 nm) core-shell particles x_v^M would decrease to 45% and to 27% with core double-shell Co(50 nm)/C(5 nm)//PS$_a$(5 nm). To be rigorous, we must say that it is a simple indication because actual systems deviate from assumptions of monodispersity or perfect 1:1 aspect ratio. It nevertheless gives first order upper limits achievable within this study. Extracted volume fraction from Fig. 4 is 34%, which is roughly consistent with these estimations.

3.4 Magnetic and electrical properties

Fig. 6 is a constitutive diagram for magnetic metal-polymer nanocomposites. It describes the cross-dependence of saturation magnetization M_s and conductivity σ that are both volume-dependent but with separate behaviors. Magnetic properties were measured by Vibrating Sample Magnetometer (VSM) and average film-conductivity was obtained with 4-point method over 25 points.

M_s is a linear function of x_v and reaches its maximum at x_v^M. Samples A1 (0.53 T, 19.3%), B4 (0.35 T, 18.1%) and B5 (0.56 T, 23.2%) are close to this maximum. This confirms that the non-covalent option is safe to the magnetization. In contrast, samples C2a (0.007 T, 2.4%), C2b (0.01T, 5.3%) are behind as *scheme 2* was not optimized and because the net-moment of Co/C has dropped ~ 70% with radicals.
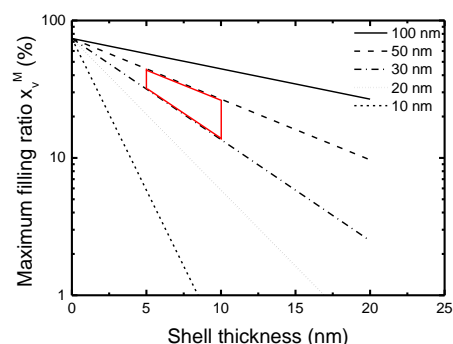
The picture is different with σ (Fig. 7). Generally, in an ideal 3D percolative system, σ is the form of $(x_v - x_{v,c})^2$ where $x_{v,c}$ is the electrical percolation threshold. Fitting equation in Fig. 6 leads to $\sigma \propto (x_v - x_{v,c})^3$ with $x_{v,c} = 2.4\%$. Exponent $t = 3$ exceeds the theoretically predicted value of 2 which is an indication of non-statistical ordered distribution of the conductive phase (*i.e.* clusters). Thus, higher exponent means that higher charge current may develop. We believe that the current flows mainly along clusters and increases the ohmic character. The current-voltage characteristic (inset Fig. 6) measured on samples B showed voltage percolation threshold at ~ 20 V. This proves that percolation sites exist, most probably between clusters.

Finally when combined with M_s, the constitutive law remains a power-function of σ with 0.2 exponent. This gives the boundary of this work indicating a preferential increase in σ before M_s. *Scheme 2* is aimed to produce less clusterized films and would give a more favorable pattern (*i.e.* lower *t*). At this stage, the combination of M_s of 0.6 to 0.9 T with σ lower than 1 S/m with *scheme 1* is unique.

To confirm the ability of the films for RF, the complex permeability was measured from 10 MHz to 10 GHz on Samples A1, B4 and B5 (Fig. 8). Results for samples of lower x_v are not presented (uncertain). The measurements were performed by high performance coil-perturbation method using impedance analyzer (Agilent 4294A) combined with vectorial network analyzer (Agilent N5222A).

Overall, the real part μ' and the imaginary μ'' are nearly constant up to 0.8 GHz with extremely low losses proving that the achieved low percolation conductivity was decisive. With A1 these characteristics extend to 10 GHz that is entirely unique. There is no sign of ferromagnetic resonance indicating that magnetocrystalline anisotropy of the particles was efficiently randomized. This remarkable feature greatly exceeds that of unsaturated magnetic materials (including ferrites) and recent works on ferrites nanocomposites [14], printable Co nanoparticles materials [4] and Co epoxy-based nanocomposites [5]. It proves that eddy currents are canceled and ferromagnetic losses are shifted until unconventional frequencies.
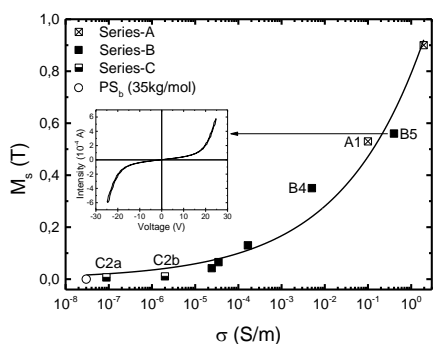
Figure 6: Cross-dependence of M_s and σ (series-A, B, C)
Inset is I-V curve of sample B5

In more details (at 1 GHz), μ' is 1.92 for A1(19.3%), 1.49 for B4(18.1%) and 1.87 for B5(23.2%). At first sight, μ' increases with x_v. Considering the losses, μ'' is $1.26.10^{-3}$ for A1(10^{-1} S/m) and $\sim 1.3.10^{-1}$ for B4(5.10^{-3} S/m) and B5(4.10^{-1} S/m). There is no clear correlation with σ. The increase of losses around 1 GHz with series-B cannot be simply linked to eddy current but also originates from magnetic domain reversal and wall propagation that may be more dissipative as the structure is imperfect. Better properties may be expected with *scheme 2* as residual clusters can be further reduced.

4   CONCLUSION

The fabrication process of non-conductive ferromagnetic films based on metal-polymer nanocomposites was described. A core double-shell structure of cobalt-graphene-polystyrene is reported able to preserve the net-moment of cobalt and to ensure electrical insulation. A thin shell of PS ($\sim$ 4 nm) was successfully grafted leading to a well-cohesive structure and preserving a high maximum filling ratio ($\sim$ 30%). The use of radicals was shown more critical, however dispersion might be improved. The percolation conductivity was discussed. Despite unfavorable percolation-pattern (clusters), we achieved low conductivity ($<$ 1 S/m) leading to extremely low losses (10^{-3}) at high frequency. To conclude we attested to the remarkable ability of such films for RF applications with a magnetization up to 0.6 - 0.9 T.
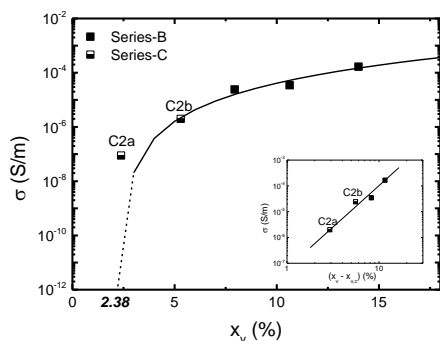
Figure 7: Dependence of σ on x_v (series-B, C)
Inset is a log-log plot
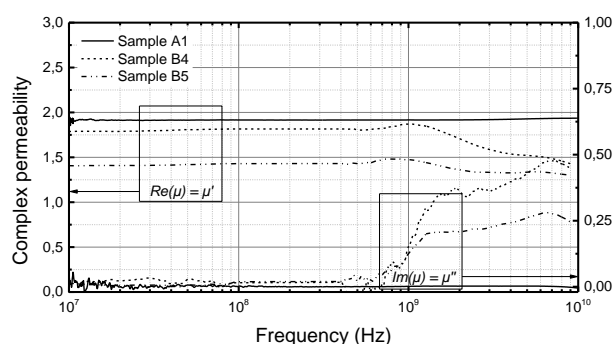
Figure 8: Complex permeability of samples A1, B4 and B5

REFERENCES

[1] D. L. Leslie-Pelecky and R. D. Rieke, Chemistry of Materials, vol. 8, pp. 1770-1783, 1996/01/01 1996.

[2] A. Hunt and R. Ewing, Percolation theory for flow in porous media vol. 771: Springer Science & Business Media, 2009.

[3] M. Varón, M. Beleggia, T. Kasama, R. J. Harrison, R. E. Dunin-Borkowski, V. F. Puntes, and C. Frandsen, Sci. Rep., vol. 3, 2013.

[4] M. Nelo, A. Sowpati, V. K. Palukuru, J. Juuti, and H. Jantunen, Progress In Electromagnetics Research, vol. 110, pp. 253-266, 2010.

[5] P. M. Raj, H. Sharma, G. P. Reddy, N. Altunyurt, M. Swaminathan, R. Tummala, and V. Nair, Journal of Electronic Materials, vol. 43, pp. 1097-1106, 2014/04/01 2014.

[6] D. A. van Leeuwen, J. M. van Ruitenbeek, L. J. de Jongh, A. Ceriotti, G. Pacchioni, O. D. Häberlen, and N. Rösch, Physical Review Letters, vol. 73, pp. 1432-1435, 1994.

[7] T. Hanemann and D. V. Szabó, Materials, vol. 3, pp. 3468-3517, 2010.

[8] T. Hayashi, S. Hirono, M. Tomita, S. Umemura, and J.-J. Delaunay, MRS Online Proceedings Library, vol. 475, pp. null-null, 1997.

[9] R. N. Grass and W. J. Stark, Journal of Materials Chemistry, vol. 16, pp. 1825-1830, 2006.

[10] R. Fuhrer, E. K. Athanassiou, N. A. Luechinger, and W. J. Stark, Small, vol. 5, pp. 383-388, 2009.

[11] V. Hermán, H. Takacs, F. Duclairoir, O. Renault, J. H. Tortai, and B. Viala, Polymer Chemistry, Submitted April 2015.

[12] T. J. Rehg and G. Higgins, AIChE Journal, vol. 38, pp. 489-501, 1992.

[13] H. Hu, X. Wang, J. Wang, L. Wan, F. Liu, H. Zheng, R. Chen, and C. Xu, Chemical Physics Letters, vol. 484, pp. 247-253, 2010.

[14] V. Castel, J. B. Youssef, and C. Brosseau, J. Nanomaterials, vol. 2007, pp. 4-4, 2007.